Bulletin of the Seismological Society of America, Vol. 88, No. 6, pp. 1457–1465, December 1998

Far-Field Radiated Energy Scaling in Elastodynamic Earthquake Fault Models

by Bruce E. Shaw

Abstract Measurements of the far-field radiated energy in very simple elastodynamic fault models is presented, and the scaling of the radiated energy with moment and rupture length is examined. The models produce a complex sequence of events having a wide range of sizes as a result of a frictional-weakening instability. Thus, radiated energy from a broad range of sizes of events can be measured. Using conservation of energy, I am able to measure the far-field energy very accurately and efficiently. I study a range of frictions, from velocity weakening to slip weakening, in order to examine the effects of the physics of the rupture source on the radiated energy. Examining the scaling of radiated energy as a function of moment and rupture length, I find differences for slip-weakening as compared to velocity-weakening friction. I find distinct differences in how the apparent stress scales with moment and also how the apparent stress divided by the stress drop scales with moment for the different frictions. Most dramatically, the apparent stress divided by the stress drop is significantly smaller for slip weakening relative to velocity weakening. This suggests that measurements of radiated energy versus moment and rupture length in earthquakes, combined with forward elastodynamic modeling, can be used to constrain possible source physics.

Introduction

What we experience as earthquakes are the dynamic elastic waves that are radiated by motions on a fault. These radiated elastic waves are perhaps the most important aspect of earthquake behavior because they are what cause nearly all of the destruction and loss of life. The radiated waves are additionally significant because, through the shaking recorded on seismograms, they provide our greatest source of quantitative measurements of earthquakes. From the point of view of trying to model earthquake behavior, trying to translate a complex physical phenomena into the language of mathematics, radiated waves are therefore a central behavior to study: It is the behavior for practical reasons we would most like to understand, and, due to the wealth of observational data, it is the behavior that provides the most constraints on theory.

The motion on the fault is also of fundamental importance. It is what causes the radiated waves, and it is the conserved quantity, the net slip across the plate boundary, that plate loading constrains. The relationship between these two fundamental quantities, radiated energy and moment, is, however, not trivial. Even in the far field, at distances large compared to the source size, the amount of radiated energy is not only a function of the net slip but also a function of how the slip occurred. Thus, the scaling of radiated energy with moment is a constraint on the possible source physics.

Measuring the total radiated energy in earthquakes is made difficult by attenuation of the energy far from the source. Thus, there is some contention as to how much energy is radiated. A number of techniques have been used and different results obtained. Teleseismic measurements of far-field *P*-wave energy by Choy and Boatwright (1995) (Boatwright, 1980, 1984) have shown very low values of radiated energy, with a roughly linear scaling of radiated energy as a function of moment. Inversion for source motions at distance to compute radiated energy has yielded conflicting estimates. Vassilou and Kanamori (1982), for example, found values consistent with the Gutenberg–Richter scaling relations of a linear radiated energy-moment trend (Gutenberg and Richter, 1956), whereas Kikuchi and Fukao (1988) found a linear trend as well, but much lower values of the radiated energy for a given moment. Direct estimates from integrating near-field records have been made by numerous authors beginning from Gutenberg and Richter (1956) and continue to be used and improved (e.g., Kanamori *et al.*, 1993). Singh and Ordaz (1994) have pointed out discrepancies between estimates using some of the different techniques. Mayeda and Walter (1996) used coda-wave envelopes to estimate energies and found a systematic increase in radiated energy with moment beyond linear scaling, with radiated energy scaling as moment to the 5/4 power. In per-

haps the cleanest measurements, due to the great depths at which the instruments were located, which reduced attenuation considerably, Abercrombie (1995) measured very low values of radiated energy for very small earthquakes. She also found what appeared to be some slight nonlinear dependence of radiated energy scaling with moment.

A thorough review of this extensive literature is beyond the scope of this article. There are, however, two things we can gleam from this abbreviated summary. First, while many studies have suggested radiated energy scales linearly with moment, some others have not. It is neither an obvious nor a necessary result, despite its simplicity. Radiated energy need not scale linearly with moment; its scaling is an interesting physical constraint on models of the source physics. Second, there have been a number of reports of very low values of radiated energy in a variety of contexts (Beroza and Jordan, 1990; McGarr, 1994), although this is also a subject of considerable discussion. This does, however, raise the question of whether some physical systems might behave this way.

What kinds of physical models produce behavior consistent with the various observations? In this letter, I present measurements of the far-field radiated energy in very simple elastodynamic models and examine the scaling of the radiated energy with moment and rupture length. Using conservation of energy, I am able to measure the far-field energy very accurately and am able to measure very small seismic efficiencies. I study a range of frictions, from velocity weakening to slip weakening, in order to examine the effects of the physics of the rupture source on the radiated energy. I find the scaling of radiated energy versus moment and rupture length, at least in these simple two-dimensional models, differs for slip-weakening as compared to velocity-weakening friction. This points to the importance of this quantity in helping distinguish observationally between different models of the source physics.

Previous Modeling Work

Various models for generating radiated energy have been proposed. There is a long history of research in which the source motions have been specified, and the resulting radiation emitted is calculated, beginning from the pioneering work of Haskell (1964) (e.g., Aki and Richards, 1980; Brune, 1970; more recently Anderson, 1997). An intermediate level of modeling where some aspects of the rupture are specified, such as the rupture propagation velocity, while other aspects are solved more dynamically, have also been studied (e.g., Andrews, 1976). Energy radiated from dynamic ruptures beginning from specified initial conditions has been studied for some time (Madariaga, 1976; Das and Aki, 1977). Recently, some fully elastodynamic methods for reconstructing near-field motions have been developed and applied to individual earthquakes (Mikumo and Miyatake, 1995; Beroza and Mikumo, 1996; Olsen *et al.,* 1997); these authors imposed various heterogeneities along the fault surface and, using slip-weakening friction, examined near-field records.

The Model

We seek to generate radiated energy from first principles, from a dynamics coupling boundary and bulk motions self-consistently. To get radiation, we need inertial dynamics, and we need a dimension perpendicular to the fault. To get a range of sizes of events, we need at least one dimension along the fault. Thus, at a minimum, we need two-dimensional elastodynamics. Here, we study one such model, introduced by (Shaw, 1997), a long two-dimensional ribbon of the scalar wave equation, bounded along one boundary by a frictional fault, and along the other by a slowly moving boundary. The slowly moving boundary represents the effect of stable creep at depth, while the frictional boundary represents the stick-slip unstably sliding fault. The wave equation couples the two surfaces elastodynamically. We nondimensionalize everything, to obtain a minimal parameterization. Mathematically, we have, in the bulk, the wave equation

$$\frac{\partial^2 U}{\partial t^2} = \nabla^2 U, \tag{1}$$

where U is the displacement field, t is time, and $\nabla^2 = \partial^2/\partial x^2 + \partial^2/\partial y^2$ is the two-dimensional Laplacian operator for the direction x, which we will take to be along the fault, and the direction y perpendicular to the fault. The wave speed is scaled to unity, so it takes unit time to travel unit length.

The fault is located at $y = 0$ with the boundary condition

$$\left.\frac{\partial U}{\partial y}\right|_{y=0} = \Phi, \tag{2}$$

where Φ is the friction. Opposite the fault is the loading surface at $y = 1$, where the boundary condition is

$$\left.\frac{\partial U}{\partial t}\right|_{y=1} = v, \tag{3}$$

where $v \ll 1$ is the slow plate-loading rate. Without loss of generality, we scale all the lengths in the problem to the distance from the fault to this loading surface, located a distance unity away. Thus, the length unity corresponds to a seismogenic fault width.

To maintain a spatially uniform fault, we use periodic boundary conditions along the fault:

$$U(x + \ell) = U(x), \tag{4}$$

where ℓ is the length of the fault. The geometry of the model

is illustrated in Figure 1. To complete the description of the model, we need to specify Φ.

All of the nonlinearity in the problem is in the friction function Φ. A central feature of the model is that in the presence of frictional weakening, when the friction decreases with increasing slip or slip rate, there is a dynamical instability in the problem, and a complex, deterministically chaotic sequence of slip events ensues. Thus, even on a fault with completely uniform material properties, an attractor nonuniform in space and nonperiodic in time results. The frictional weakening is a crucial ingredient in obtaining the complexity: Friction that only strengthens, increasing with slip or slip rate, leads to noncomplex periodic solutions. There are both similarities and differences in the behavior that arises from different kinds of frictional weakening. We therefore want to study a range of frictions and compare the resulting behavior.

The form of the friction Φ we examine in this article is chosen for two reasons. One is mathematical: it encompasses a range of frictional-weakening mechanisms, from slip to velocity weakening. The other motivation is physical: The form represents a simple quantification of a physical idea that goes back to Sibson (1973), that heat from frictional sliding will raise the temperature and, therefore, the pressure of pore fluids, thereby decreasing the effective normal stress and therefore friction. If the dissipation of heat is taken to occur over some time scale, then slip weakening results if the dissipation is slow compared to the rupture time scale (Lachenbruch, 1980), and velocity weakening results if the dissipation is fast compared to the rupture time scale (Shaw, 1995). The friction used here is the same as in Shaw (1997), where it is discussed in more detail.

There are four aspects to the friction. First, it is a stick-slip friction, which resists motion up to some threshold value. Second, there is a rapid drop in friction once sliding begins. Third, there is a slower overall weakening that depends on some mixture of slip and slip rate. Fourth, there is a viscous term, which stabilizes the small scales. In a general form, we represent the friction as

$$\Phi = \phi\left(\frac{\partial S}{\partial t'},\ t' \leqq t\right) H\left(\frac{\partial S}{\partial t}\right) - \eta\nabla_{\|}^2 \frac{\partial S}{\partial t}. \qquad (5)$$

Here

$$\frac{\partial S}{\partial t} = \left.\frac{\partial U}{\partial t}\right|_{y=0}$$

is the slip rate on the fault, with ϕ depending on the past history of slip. The function H is the antisymmetric step function, with

$$H = \begin{cases} \dfrac{\widehat{\partial S}}{\partial t} & \dfrac{\partial S}{\partial t} \neq 0, \\ |H| < 1 & \dfrac{\partial S}{\partial t} = 0, \end{cases} \qquad (6)$$

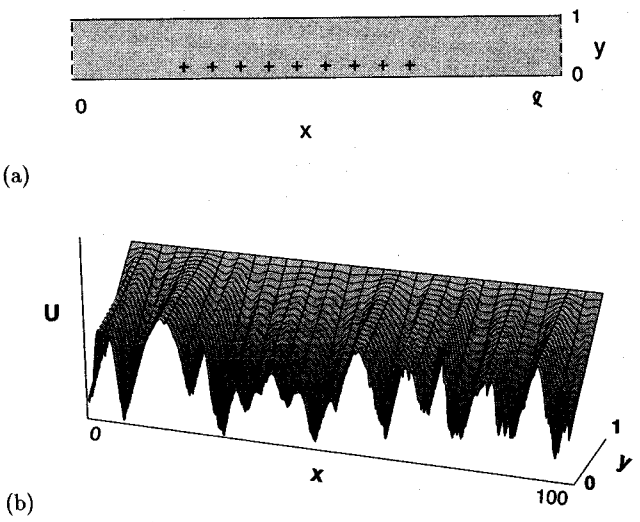

Figure 1. Geometry of the model. (a) The long cylindrical geometry of the space (rectangular, with periodic boundary conditions denoted by dashed lines). The fault is located at $y = 0$, while the slowly loaded driving surface is located parallel to the fault, a distance unity away at $y = 1$. The (+) symbols represent the locations of an array of velocity-meters placed near the fault. (b) The geometry of a typical solution for the displacement U. There is constant displacement along the loading surface at $y = 1$ and irregular displacements that have developed along the fault at $y = 0$. The wave equation connects the two boundaries; in this example, where the fault is stuck, the acceleration is zero on the interior, and the Laplacian operator smoothly interpolates between the two boundaries. The x axis is compressed relative to the y axis in the figure; the aspect ratio $\ell = 100$ in this example.

where $\widehat{\partial S/\partial t}$ is the unit vector in the sliding direction. Thus, H represents the stick-slip nature of the friction, being multivalued at zero slip rate.

The parameter η is a constant that sets the amount of viscosity and sets the scale at which the small wavelengths are stabilized. The subscript on the viscous term Laplacian denotes that it is the derivative parallel to the fault, which gives $\nabla_{\|}^2 = \partial^2/\partial x^2$ for the geometry we consider here in equation (2) (Langer and Nakanishi, 1993).

We choose the particular form for the history dependence of ϕ taken in this article for two reasons. First is its simplicity. Second, it is motivated by a physical picture of how frictional heating can produce frictional weakening. We use

$$\phi = \Phi_0 - \sigma - \frac{\alpha Q}{1 + |\alpha| Q}. \qquad (7)$$

The first term Φ_0 is a constant that sets the sticking threshold. It turns out to be an irrelevant parameter in the problem, as long as it is large compared to the maximum friction drop,

so as to prevent back slipping. Thus, only stress drops matter in the dynamics, not total stress. Φ_0 does affect the heat generated, but that is an effect we will consider here only indirectly, insofar as it feeds back and affects the friction.

There is one other symmetry in the problem that we have used. The symmetry is the rescaling of the equations of motion, which remain invariant under a rescaling of U, Φ, and v by the same constant. Thus, without loss of generality, we have set the stress change of the last term in (7) to unity and scaled all the other stresses to this stress change.

For the second term σ, which represents the rapid drop in friction that occurs in going from sticking to sliding friction, we make a major departure from how usual friction behaves and make it a time-dependent function:

$$\sigma = \begin{cases} \sigma_0 \dfrac{t - t_s}{\tau} & t - t_s < \tau, \\ \sigma_0 & t - t_s \geqq \tau, \end{cases} \tag{8}$$

so that σ increases linearly with time once the fault becomes unstuck, up to a maximum value σ_0 over a time scale τ, and is reset to zero when the fault resticks. The time t_s is measured from the last unsticking and is reset during an event if the fault resticks and then slips again. This term neglects all the complicated rate- and state-dependent effects that are observed to accompany the nucleation of slip in laboratory friction experiments (Dieterich, 1979, 1992; Blanpied *et al.*, 1991). We do this for two reasons. First, it allows us to take the limit of the loading rate $v \to 0$, so that this parameter is irrelevant to the dynamics, and only sets the time scale between events. Consequently, we have a much more efficient numerical algorithm. Second, many of the aspects of small events do not depend on the details of the nucleation process, and we would like to use as simple a system as is valid for what we are interested in. Our claim is not that this is the most realistic description of nucleation but, that the properties of the system we are measuring in this article are not sensitive to the details of the nucleation mechanism.

The third term in equation (7) contains the key dependence on slip and slip rate in the friction, through the variable Q. The variable Q is something like heat, which accumulates with increasing slip rate and dissipates on a time scale $1/\gamma$:

$$\frac{\partial Q}{\partial t} = -\gamma Q + \left|\frac{\partial S}{\partial t}\right|. \tag{9}$$

The dissipation with γ gives a simple, physically motivated healing mechanism, which also turns out to give a nice range of properties.

An equivalent integral solution of Q,

$$Q(t) = \int_{-\infty}^{t} e^{-\gamma(t-t')} \left|\frac{\partial S}{\partial t'}\right| dt', \tag{10}$$

shows that when γ is small compared to unity, the inverse rupture time scale, Q is just the slip in an event, while when $\gamma \gg 1$, Q is $1/\gamma$ times the slip rate.

The constant α sets the slope of the stress drop with heat Q, with $\alpha > 0$ giving weakening with Q, and $\alpha < 0$ giving strengthening with Q. This parameter plays a crucial role in the problem. Because Q is nonnegative, the denominator in equation (7) only gets larger with Q, eventually saturating the change with αQ.

Further discussion of the physical motivations behind this formulation of friction can be found in (Shaw, 1995, 1997). What is convenient for us in this article is that we can study a range of types of weakening, with slip weakening and velocity weakening as end-member cases, by varying the parameter γ.

The fault remains stuck until the stresses reach the maximum sticking threshold, whereupon sliding commences. Beginning from any nonconstant initial condition, when there is frictional strengthening, nothing interesting happens, and a periodic solution develops. In contrast, when there is frictional weakening, there is an instability, and a complex sequence of events develops. Figure 2 shows an example of a complex sequence that has developed in the weakening case. Two different ways of looking at the same sequence of events are shown. In Figure 2a, we plot the times at which various points along the fault have slipped. In Figure 2b, we plot the net slip when the fault is at rest.

There are a variety of ways of quantifying the complex behavior that develops in the elastodynamic models; previous work has examined the distribution of sizes of events (Carlson and Langer, 1989), the correlations of small events with upcoming large events (Shaw *et al.*, 1992; Pepke *et al.*, 1994), the moment source spectra (Shaw, 1993), and the scaling of moment with source length (Myers *et al.*, 1996), among other things. In this letter, I consider a new quantification of behavior of these complex events, the radiated energy in the far field.

Results

Motions on the fault cause motions in the bulk. In the near field, much of the kinetic energy goes to rearranging the displacement field and thereby goes into rearranging the potential energy density. Only some of the kinetic energy manages to escape to the far field and is radiated away. One way to visualize the near-field motions is with an array of velocity records. Taking an array of records located near but off the fault and spaced evenly along the fault, as indicated in Figure 1a, we can observe the coherent motions created by an event. Figure 3 shows two events, one small (Fig. 3a) and one large (Fig. 3b). The small event illustrates a sort of empirical Greens function for the medium. The horizontal axis is time, and the vertical axis is velocity, v = ∂U/∂t, with neighboring velocity records offset vertically by a constant amount. We see an initial short-velocity pulse, corresponding to the short event, followed later by a broad

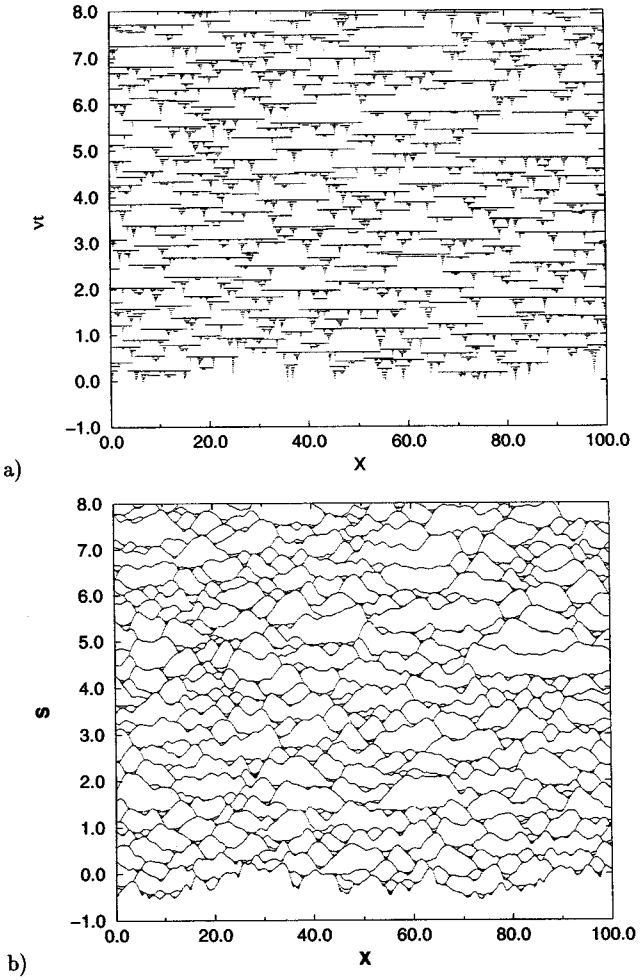

Figure 2. Two different ways of looking at a sequence of events that has developed in a weakening case. The horizontal axes are distance along the fault. The vertical axes are (a) the time at which different portions of the fault have slipped, and (b) the net slip in the stuck configuration. The same sequence of events is shown in Figures a and b. The parameter values used in this figure are $\alpha = 4$, $\gamma = 1$, $\sigma_0 = 0.03$, $\tau = 0.1$, $\eta = 0.005$, and $\delta_x = 0.1$.

reflection of the waves scattering off of the stiff, slowly moving boundary a distance unity from the fault. A large event is shown in Figure 3b, with a decreased magnification of the time and velocity axes. We see the relatively messy epicentral region organizing into two large pulses of slip emanating bilaterally down the fault. The pulse traveling down the page dies out, while the pulse traveling up the page continues on, and dies later, beyond the array. Coherent packets of scattered energy ring on behind the passage of the main rupture pulses.

This visualization provides a qualitative picture of some of the complex spatial and temporal aspects of the radiative field in the bulk. To provide a more quantitative measure of the behavior, we step back to the far field.

One could measure, directly, the far-field radiated energy by integrating the energy flux through a far surface that enclosed the source. One would, however, have to wait a long time for the waves to travel to the far surface and for all the scattered waves to finish passing through it. I circumvent this difficulty by using conservation of energy. I keep track of the work done on the boundaries, which, because there is no work done at the far boundary during an event (in the limit as $v \to 0$, as we use here), is just the work done on the fault:

$$W = \int \Phi \frac{\partial U}{\partial t} \, dxdt. \tag{11}$$

I also calculate the potential energy P

$$P = \int \frac{1}{2} (\nabla U)^2 dV \tag{12}$$

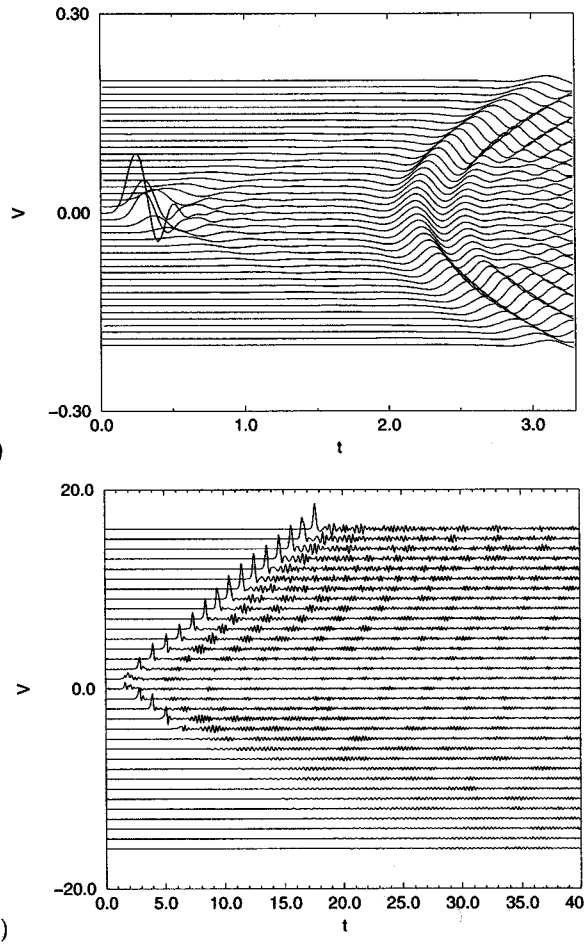

Figure 3. An array of near-field velocity records for (a) a small and (b) a large event. Note the difference in velocity scale on the vertical axis and a difference in the time scale on the horizontal axis in the two plots.

in the static solution before and after the event (V is the volume). Then the difference between the potential energy before and after an event, ΔP, minus the work done on the fault is the radiated energy E, because there are no other energy sources or sinks in the model (i.e., no dissipation in the bulk):

$$\Delta P - W = E. \tag{13}$$

This conservation of energy method works because we are solving things in a consistent dynamic—as opposed to kinematic—way.

There are a few other quantities that need defining. The Moment M of an event is the net slip on the surface

$$M = \int \delta U(x)dx, \tag{14}$$

where $\delta U(x) = U(x,t_f)|_{y=0} - U(x,t_0)|_{y=0}$ is the slip on the fault in an event, the difference in displacement between the initial time t_0 at the start of an event and the final time t_f when the event is finished.

The length L of an event is the net length of the fault that slipped:

$$L = \int \theta[\delta U(x)]dx, \tag{15}$$

where $\theta = 1$ if the fault slipped, and $\theta = 0$ otherwise.

In our dimensionless units, the apparent stress σ_a is defined by Wyss and Brune (1968):

$$E = \sigma_a M. \tag{16}$$

The stress drop $\Delta\sigma$ depends on the slip and rupture length and has some fault dimension dependence:

$$\Delta\sigma = M/L^{\eta} \tag{17}$$

with $\eta = 3$ for earthquakes in three dimensions, and $\eta = 2$ in two dimensions, which we study here. This expression for stress drop neglects finite-depth effects occurring at large rupture lengths, but it is simple and sufficient for our purposes.

To check the consistency of the methodology, I have done a number of tests. First, I have checked that the results are independent of the spatial grid resolution and temporal time-step resolution. Second, I have tested the method on a reduced one-dimensional model, where the loading boundary is only one grid-element away [the model of Burridge and Knopoff (1967)], and measured that indeed, as expected, there is no radiated energy (to the resolution of 10^{-6} of the method). Third, I have checked that the radiated energy is independent of the absolute level of stress and only depends on the stress drop; changing Φ_0 leaves the results unchanged. Fourth, I have checked that in the limit where the friction drops very rapidly with time to a nearly constant value, when $\sigma_\tau \gg \sigma_Q$ and $\tau \ll 1$, the apparent stress σ_a approaches the stress drop $\Delta\sigma$ as expected. Finally, though it is much less efficient and only approximately accurate, I have done a further numerical check on the results by looking at the time integral of the square of the velocity on two bounding planes, on both sides and away from the rupture, which go from the fault at $y = 0$ to the far edge at $y = 1$. (Because the boundary opposite the fault is steady, no energy is radiated through it.) This gives an approximate estimate (neglecting angle of incidence) of the radiated energy by a completely independent method. The results are consistent with the conservation of energy approach.

Our first set of results are shown in Figure 4. This shows the radiated energy E, as a function of moment M, for different values of the parameter γ going from slip weakening at small γ to velocity weakening at large γ. Each point corresponds to an individual event, with the different symbols representing different values of γ. In this plot, and the plots that follow, we fix $\sigma_0 = 0.03$ and $\tau = 0.1$. Note that there are significant differences between slip and velocity weak-

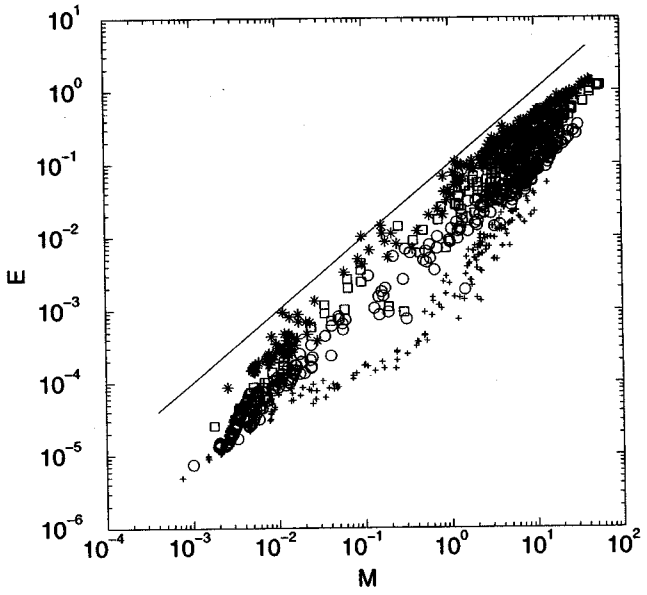

Figure 4. Radiated energy E versus moment M, comparing different-sized events and different amounts of velocity versus slip weakening. Each point in the plot corresponds to an individual event. The different symbols correspond to different friction parameters. For the velocity-weakening cases, we vary γ while keeping α/γ fixed, at a value of 3. For these cases, the symbols are (○) for $\gamma = 1$, (□) for $\gamma = 10$, and (*) for $\gamma = 100$. The (+) symbol corresponds to the slip-weakening case, with $\alpha = 3$ and $\gamma = 0.1$. Increasing γ corresponds to increasing the amount of velocity weakening. Note the increased apparent stress $\sigma_a = E/M$ for bigger γ. Note also that for large values of γ, E scales linearly with M; the solid line, for comparison, shows a linear scaling of E versus M,with apparent stress $\sigma_a = 0.1$.

ening. Larger values of γ, more velocity weakening, gives more E for a given M. Small values of γ, slip weakening, gives very little radiation, and a nonlinear scaling of E with M. This suggests apparent stress as a function of moment may be a useful quantity in trying to distinguish different source physics. Let us push this question further and look at other scaling laws.

Figure 5 shows moment M as a function of rupture length L, for the slip- and velocity-weakening cases. In contrast with the previous figure, the differences between these two types of frictional weakening here appear relatively subtle. Thus stress drop as a function of moment does not appear to be very useful, in this case, in distinguishing between the different source physics.

What happens when we combine the two types of stress and plot apparent stress versus stress drop (Savage and Wood, 1971; Abercrombie, 1995)? Figure 6 shows this plot for the model data, and the two types of friction, slip weakening and velocity weakening. The striking differences between the two frictions on this plot suggests this may potentially be an excellent way of distinguishing the source physics. Note that the two types of frictions collapse into two quite distinct sets, with the velocity-weakening data clustering near the line where $\sigma_a = \Delta\sigma$. In contrast, the slip-weakening shows σ_a being an order of magnitude smaller than $\Delta\sigma$. This is a significant, potentially observable difference. How does this compare with real earthquakes? Both E and L are difficult to measure accurately, so there are large uncertainties in the real data. Abercrombie (1995) used deep borehole measurements that had the advantage of minimizing attenuation effects. Though her data come from only a relatively narrow magnitude range, it is useful to compare the earthquake data with the model. In Abercrombie (1995, Fig. 12), we see remarkable similarities in both the relative values of σ_a to $\Delta\sigma$ and in the scatter, compared to the slip-weakening case here. Both show σ_a being about a factor of 10 smaller than $\Delta\sigma$. (The axes on her figure and the figure here are reversed.) This is an important number. It says earthquakes are relatively quite quiet. They could shake an order of magnitude harder and still have no problems with their energy budgets. Velocity weakening, in contrast, appears to be much louder. Due to the uncertainties in the earthquake measurements, the low dimensionality of the models, and the restricted range of the friction studied, one should be cautious about pushing these quantitative comparisons too far at this point. Nonetheless, this does appear to be a potentially extremely useful plot to quantify the behavior and distinguish between different models of the source physics.

While the plot of apparent stress versus stress drop appears to be quite useful, we can go further and note that there is additional information potentially available in the data. In

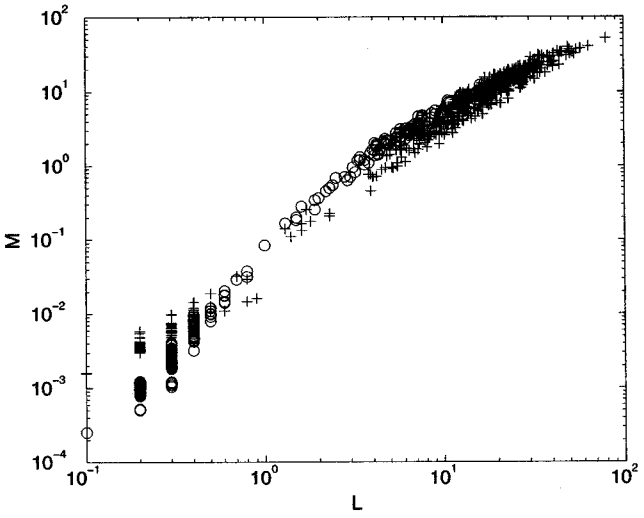

Figure 5. Moment M versus length of rupture L, comparing different-sized events and different frictions. Two different frictions, slip weakening denoted with the (○) symbol and velocity weakening denoted with the (+) symbol, are shown. The parameters are $\alpha = 6$, $\gamma = 0.1$, and $\alpha/\gamma = 6$, $\gamma = 10$, respectively. Each point in the plot corresponds to an individual event. Note that there are differences between the two frictions but only relatively subtle ones.

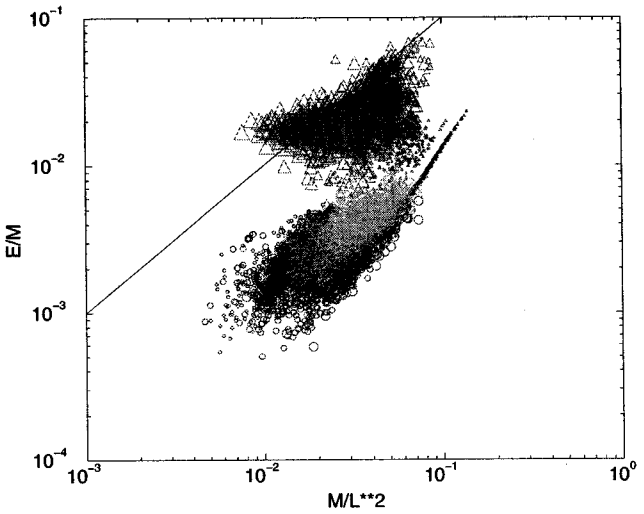

Figure 6. Apparent stress vs. stress drop. Each point in the plot corresponds to an individual event. There are two types of friction shown, with slip weakening denoted by a (○) symbol, and velocity weakening denoted with a (Δ) symbol. The parameters are $\alpha = 6$, $\gamma = 0.1$, and $\alpha/\gamma = 6$, $\gamma = 10$, respectively. The size of the symbols are scaled with the magnitude of the events, with the largest events having the largest symbol size. There is an additional redundant gray scale indicating the magnitude as well, with the lighter color for a given symbol being larger. Note the complete separation of the two populations, with the slip weakening showing an order of magnitude lower apparent stress to stress drop ratio. The solid line indicates the line where apparent stress equals stress drop.

particular, there may be a magnitude dependence to the dependence of the apparent stress on stress drop. Following Savage and Wood (1971), we define a measure of earthquakes, a dimensionless number we will call the earthquake loudness, which is the ratio of the two stresses:

$$\varepsilon \equiv \frac{\sigma_a}{\Delta\sigma} = \frac{E/M}{M/L^D}, \tag{18}$$

with $D = 2$ here in this 2D model. Savage and Wood (1971) examined very simple ruptures and found bounds on ε of order unity. Because of the approximate way we are estimating stress drop in equation (17), however, for large events, when $L \gg 1$, we can get values of ε exceeding unity. Nonetheless, this is a useful measure for comparison. Figure 7 shows these results of ε as a function of moment M. Again, we see significant differences between slip and velocity weakening. Again, the velocity weakening is much louder than the slip weakening. We also see a difference in how loudness changes: slip weakening shows ε decreasing with M for small events, while velocity weakening shows ε increasing with M for small events. This appears to be a very promising measurement to attempt to make with real earthquake data.

How robust are these results? Changing the grid resolution does not affect things. Changing τ and σ (as long as it is not too large) do not change things much. If we replace the time-dependent σ we use here with a σ that has only a very small time-dependent part, along with a part similar to the Q-dependent part of the friction, but with a larger slope, things are unchanged for the velocity-weakening case, while for the slip-weakening case, the small events are somewhat quieter still. Changing α (as long as it is not too small) does not have much effect over the range we can vary it. Changing η does have some quantitative though not qualitative effect. Changing η changes the small length scale above which the friction becomes unstable. Thus, changing η affects the sharpness of the rupture pulses, with smaller η giving smaller unstable length scales. The effect on the radiated energy is primarily seen in the smallest and largest events, with larger η leading to slightly smaller loudness ε for these events. In summary, for the frictions we have studied, the results are quite robust.

I have, additionally, checked whether the overall geometry of the system is important. I have carried out the measurements using an alternative two-dimensional crustal plane geometry where the loading was placed in the bulk rather than on the boundary as in (1). This gives the Klein Gordon equation for the bulk dynamics (Myers *et al.*, 1996); equation (1) is replaced by

$$\frac{\partial^2 U}{\partial t^2} = \nabla^2 U + vt - U. \tag{19}$$

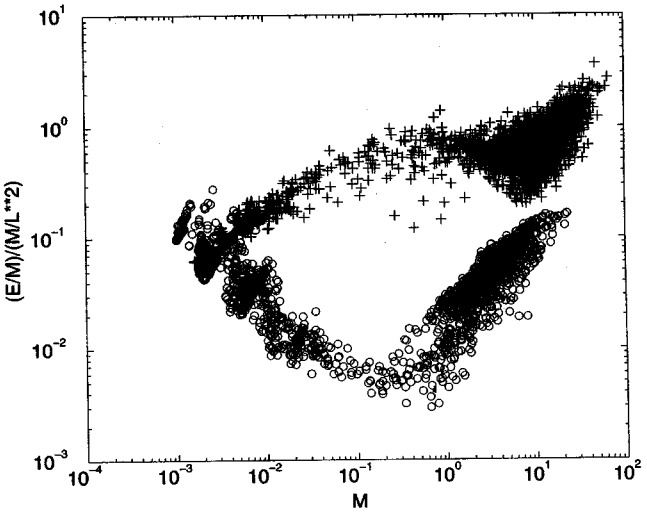

Figure 7. Apparent stress to stress drop ratio ε as a function of moment M, comparing different sized events and different amounts of velocity versus slip weakening. Each point in the plot corresponds to an individual event. The different symbols correspond to different friction parameters. The (○) symbol corresponds to the slip-weakening case, with $\alpha = 6$ and $\gamma = 0.1$. The (+) symbol corresponds to the velocity-weakening case, with $\alpha/\gamma = 6$ and $\gamma = 10$. Note that for the small events with slip weakening, the loudness ε decreases with increasing moment. In contrast, for the velocity-weakening case, it increases slightly.

Using the same frictions on that two-dimensional model as here, the results look the same.

Conclusion

The puzzle of small apparent stress has been pointed to for a long time (e.g., Kanamori, 1994). Here, I have shown that they can arise naturally in the context of elastodynamics with friction. In particular, slip-weakening friction was seen to have a low apparent stress to stress drop ratio, a ratio of order 1/10. Velocity weakening, in contrast, was seen to have a ratio closer to unity. More generally, we can ask what scaling relations show differences between slip and velocity weakening, and, therefore, which ones may help us place constraints on possible source physics. This loudness ratio of apparent stress to stress drop was thus seen to be a good measure to distinguish slip weakening from velocity weakening. In contrast, measurements of stress drop alone from moment-rupture length scaling showed little difference between slip and velocity weakening. Some difference in apparent stress versus moment was seen, so that may be a useful measure. A clear difference was seen in plots of loudness versus moment, suggesting that this would be a useful plot to examine in real earthquake data.

By finding significant differences in the behavior of different types of friction, this work suggests measurements of

radiated energy in earthquakes, combined with forward elastodynamic modeling, can be used to constrain possible source physics. It supports continued efforts to improve and reconcile the different and difficult measurements.

Much discussion in self-organizing models has focussed on the question of what is the distribution of sizes of events. Independent of that issue, however, is the very important question of what the events themselves look like. In this letter, I have examined, qualitatively, coherent near-field velocities and, quantitatively, far-field radiated energies. This work opens up new axes to compare self-organizing models with observations, where there is potentially a vast amount of observational constraints, and with potentially great practical uses.

Acknowledgments

Alexei Tumarkin and an anonymous referee provided helpful reviews. This work was supported by NSF Grant 94-17700 and USGS Grant 1434HQ97GR03074. LDEO contribution #5873.

References

Abercrombie, R. E. (1995). Earthquake source scaling relationships from -1 to 5 M_L using seismograms recorded at 2.5-km depth, *J. Geophys. Res.* **100,** 24015.

Aki, K. and P. Richards (1980). *Quantitative Seismology: Theory and Methods,* W. H. Freeman, New York.

Anderson, J. G. (1997). Seismic energy and stress-drop parameters for a composite source model, *Bull. Seism. Soc. Am.* **87,** 85.

Andrews, D. J. (1976). Rupture propagation with finite stress in antiplane strain, *J. Geophys. Res.* **81,** 3575.

Beroza, G. C. and T. H. Jordan (1990). Searching for slow and silent earthquakes using free oscillations, *J. Geophys. Res.* **95,** 2485.

Beroza, G. C. and T. Mikumo (1996). Short slip duration in dynamic rupture in the presence of heterogeneous fault properties, *J. Geophys. Res.* **101,** 22449.

Blanpied, M. L., D. A. Lockner, and J. D. Byerlee (1991). Fault stability inferred from granite sliding experiments at hydrothermal conditions, *Geophys. Res. Lett.* **18,** 609.

Boatwright, J. (1980). A spectral theory for circular seismic sources: Simple estimates of source dimension, dynamic stress drop and radiated seismic energy, *Bull. Seism. Soc. Am.* **70,** 1.

Boatwright, J. (1984). Seismic estimates of stress release, *J. Geophys. Res.* **89,** 6961.

Brune, J. N. (1967). Tectonic stress and spectra of seismic shear waves from earthquakes, *J. Geophys. Res.* **75,** 4997.

Burridge, R. and L. Knopoff (1967). Model and theoretical seismicity, *Bull. Seism. Soc. Am.* **57,** 341.

Carlson, J. M. and J. S. Langer (1989). Mechanical model of an earthquake fault, *Phys. Rev. A* **40,** 6470.

Choy, G. L. and J. Boatwright (1995). Global patterns of radiated seismic energy and apparent stress, *J. Geophys. Res.* **100,** 18295.

Das, S. and K. Aki (1977). fault plane with barriers: a versatile earthquake model, *J. Geophys. Res.* **82,** 5658.

Dieterich, J. H. (1979). Modeling of rock friction: 1. Experimental results and constitutive equations, *J. Geophys. Res.* **84,** 2161.

Dieterich, J. H. (1992). Earthquake nucleation on faults with rate and state dependent strength, *Tectonophysics* **211,** 115.

Gutenberg, B. and C. F. Richter (1956). Earthquake magnitude, intensity, energy, and acceleration, *Bull. Seism. Soc. Am.* **46,** 105.

Haskell, N. (1964). Total energy and energy spectral density of elastic wave radiation from propagating faults, *Bull. Seism. Soc. Am.* **54,** 1811.

Kanamori, H., J. Mori, E. Haukson, T. H. Heaton, L. K. Hutton, and L. M. Jones (1993). Determination of earthquake energy release and M_L using TERRAscope, *Bull. Seism. Soc. Am.* **83,** 330.

Kanamori, H. (1994). Mechanics of earthquakes, *Ann. Rev. Earth Planet. Sci.* **22,** 207.

Kikuchi, M. and Y. Fukao (1988). Seismic wave energy inferred from long-period body wave inversion, *Bull. Seism. Soc. Am.* **78,** 1707.

Lachenbruch, A. (1980). Frictional heating, fluid pressure, and the resistance to fault motion, *J. Geophys. Res.* **85,** 6097.

Langer, J. S. and H. Nakanishi (1993). Models of crack propagation II: two dimensional model with dissipation on the fracture surface, *Phys. Rev. E* **48,** 439.

Madariaga, R. (1976). Dynamics of an expanding circular fault, *Bull. Seism. Soc. Am.* **66,** 639.

Mayeda, K. and W. R. Walter (1996). Moment, energy, stress drop, and source spectra of western United States earthquakes from regional coda envelopes, *J. Geophys. Res.* **101,** 11195.

McGarr, A. (1994). Some comparisons between mining-induced and laboratory earthquakes, *Pageoph* **142,** 467.

Mikumo, T. and T. Miyatake (1995). Heterogeneous distribution of dynamic stress drop and relative fault strength recovered from the results of waveform inversion: the 1984 Morgan Hill California earthquake, *Bull. Seism. Soc. Am.* **85,** 178.

Myers, C. R., B. E. Shaw, and J. S. Langer (1996). Slip complexity in a crustal plane model of an earthquake fault, *Phys. Rev. Lett.* **77,** 972.

Olsen, K. B., R. Madariaga, and R. J. Archuleta (1997). Three-dimensional dynamic simulation of the 1992 Landers earthquake, *Science* **278,** 834.

Pepke, S. L., J. M. Carlson, and B. E. Shaw (1994). Prediction of large events on a dynamical model of a fault, *J. Geophys. Res.* **99,** 6769.

Savage, J. C. and M. D. Wood (1971). The relation between apparent stress and stress drop, *Bull. Seism. Soc. Am.* **61,** 1381.

Shaw, B. E. (1993). Moment spectra in a simple model of an earthquake fault, *Geophys. Res. Lett.* **20,** 643.

Shaw, B. E. (1995). Frictional weakening and slip complexity on earthquake faults, *J. Geophys. Res.* **100,** 18239.

Shaw, B. E. (1997). Modelquakes in the two dimensional wave equation, *J. Geophys. Res.* **102,** 27367.

Shaw, B. E., J. M. Carlson, and J. S. Langer (1992). Patterns of seismic activity preceding large earthquakes, *J. Geophys. Res.* **97,** 479–488.

Sibson, R. H. (1973). Interactions between temperature and pore fluid pressure during earthquake faulting and a mechanism for partial or total stress relief, *Nature Phys. Sci.* **243,** 66.

Singh, S. K. and M. Ordaz (1994). Seismic energy release in Mexican subduction zone earthquakes, *Bull. Seism. Soc. Am.* **84,** 1533.

Smith, K. D., J. N. Brune, and K. F. Priestley (1991). The seismic spectrum, radiated energy, and the Savage and Wood inequality for complex earthquakes, *Tectonophysics* **188,** 303.

Vassilou, M. S. and H. Kanamori (1982). The energy release in earthquakes, *Bull. Seism. Soc. Am.* **72,** 371.

Wyss, M. and J. N. Brune (1968). Seismic moment, stress, and source dimensions for earthquakes in the California-Nevada region, *J. Geophys. Res.* **73,** 4681.

Lamont-Doherty Earth Observatory
Columbia University
Palisades, New York 10964
E-mail: shaw@ldeo.columbia.edu

Manuscript received 10 December 1997.